Dense particle cloud dispersion by a shock wave

M. Kellenberger, C. Johansen*, G. Ciccarelli, F. Zhang**

Queen's University
Mechanical and Materials Engineering
Kingston, Ontario, K7L 3N6, Canada
kellenbergerm@me.queensu.ca

*University of Calgary
Mechanical and Manufacturing Engineering
Calgary, Alberta, T2N 1N4, Canada

**Defense Research and Development Canada - Suffield
Medicine Hat, Alberta, T1A 8K6, Canada

Abstract

A dense particle flow is generated by the interaction of a shock wave with an initially stationary packed granular bed. High-speed particle dispersion research is motivated by the energy release enhancement of explosives containing solid particles. The initial packed granular bed is produced by compressing loose powder into a wafer with a particle volume fraction of $\Phi = 0.48$. The wafer is positioned inside the shock tube, uniformly filling the entire cross-section. This results in a clean experiment where no flow obstructing support structures are present. Through high-speed shadowgraph imaging and pressure measurements along the length of the channel, detailed information about the particle shock interaction was obtained. Due to the limited strength of the incident shock wave, no transmitted shock wave is produced. The initial “solid-like” response of the particle wafer acceleration forms a series of compression waves that eventually coalesce to form a shock wave. Breakup is initiated along the periphery of the wafer as the result of shear that forms due to the fixed boundary condition. Particle break-up is initiated by local failure sites that result in the formation of particle jets that extend ahead of the accelerating, largely intact, wafer core. In a circular tube the failure sites are uniformly distributed along the wafer circumference. In a square channel, the failure sites, and the subsequent particle jets, initially form at the corners due to the enhanced shear. The wafer breakup subsequently spreads to the edges forming a highly non-uniform particle cloud.

Introduction

The study of particle cloud dispersion by a shock wave is important to many applications. For example, the propagation of shock wave through a dusty gas has been studied for many years [1]. In these studies the particle volume fraction is insignificant and the particle acceleration can be modeled using simple drag correlations based on a solid sphere in an infinite fluid medium. A modern application includes multiphase explosives that comprise of a condensed explosive surrounded with packed micrometric reactive metal particles. The particle dispersion in this application is very complicated as the particle flow interaction transitions through multiple regimes, each requiring a different treatment. The solid volume fraction, Φ, of the flow is used to identify the regimes [2]. In a granular bed ($\Phi >$ \$0.5), forces are exerted also through direct contact of the closely packed particles. In a dilute gas-solid flow ($\Phi <$

0.01), the effects of particle collisions become negligible. Between these two regimes is a dense gas-solid flow ($0.1 < \Phi < 0.5$). Detonation of the explosive generates a shock wave which accelerates and compacts the particles and when the shock reaches the particle layer outer boundary a reflected expansion wave further accelerates the particles. The shock wave initially propagates through a granular particle bed and much later after the passage of the shock wave, the particles are further dispersed by the radial combustion product flow forming a cloud. In this application it is important to understand the dispersion of the particles as the energy release from the particles maintains the pressure in the shock sphere, thereby increasing the shock wave impulse [3]. The particle dispersion phenomenon varies from early time when the particle volume fraction is large, to later time where the volume fraction is very small and the flow is considered a dilute gas-solid flow, i.e., similar to a dusty-gas flow. The particle dispersion phenomenon responsible for very late time dispersion has been studied extensively in the past and is relatively well understood. However, for the early time dispersion of a granular bed, as the particle cloud expands, a dense gas-solid flow exists which has not received much attention and is not very well understood [2].

Reactive multiphase flow models have been used to simulate the acceleration and dispersion of the particle cloud that occurs in multiphase explosives [4]. The fidelity of the simulations is severely limited by the physical drag models that take into account the interactions in the dense gas-solid flow [2]. In order to develop an accurate particle drag model that describes particle acceleration in the dense flow regime, representative experimental data need to be generated. Large-scale experiments have been carried out with spherical multiphase explosive charges to visualize the global particle cloud dispersion [5]. Controlled shock wave experiments are necessary to gain understanding of the fundamental physics of the dense supersonic gas-solid flow interactions and obtain quantitative data concerning the particle cloud dispersion. Shock tube experiments have been carried out in the past but typically the particle suspension method influences the shock flow [4] and the particle size is not typical of multiphase explosives. Recently shock tube experiments were carried out by Wagner et al. [6] looking at the interaction of a shock wave and a gravity-fed particle "curtain." The roughly 3 mm thick particle curtain, consisting of 100 micron sized soda lime particles, had an estimated particle volume fraction of $\Phi = 0.15$, which is in the dense gas-solid flow regime. Schlieren photography was used to visualize the interaction of the particle curtain with 1.67 and 1.95 Mach number shocks. The dispersion was characterized by tracking the downstream and upstream edges of the particle cloud. The videos show that the interaction of the shock wave with the particle curtain produces a transmitted and reflected shock wave. Immediately following the shock interaction the particle cloud accelerates and grows axially. The cloud dispersion was found to be exactly the same for both shock strengths tested. The particle curtain only extended 87% of the full 76 mm width of the channel. As will be discussed later, the gap between the particle curtain and the shock channel glass side-wall is necessary to prevent sticking of the particles and the subsequent obscuring of the cloud upstream edge. The drawback is that the gaps on either side of the curtain introduce three-dimensional effects. For example, diffraction of the incident shock wave past the gap shows up as thickening of the shock wave in the schlieren image [6].

This paper reports on shock tube experiments looking at the acceleration and dispersion of 100 micron-sized aluminum oxide particles [7]. By pure coincidence the experimental conditions are very similar to those of the Wagner et al. experiment, i.e., similar shock tube cross-section dimensions, shock wave strength, and particle size. The main difference between the experiments is in the initial particle cloud volume density. The novel feature of the present experiments is the initial configuration of the particles in the form of a free-standing wafer covering the entire shock tube cross-section. This method allows absolute control over the initial particle distribution without the use of flow obstructing structures.

Experimental

The shock tube consists of a 1.96 m long, 10 cm diameter driver, a transition section, and a driven section consisting of five 0.6 m long, 7.6 cm square sections as shown in Fig. 1 The transition section is 0.75 m long. Some experiments used a 6.99 cm inner-diameter acrylic tube inserted into the channel to obtain a circular cross-section. A double diaphragm is used to precisely control the driver pressure at the time of diaphragm rupture. Helium (298 K) is used in the driver and atmospheric air is used in the driven section. Piezoelectric pressure transducers are flush-mounted on the top surface of the driven section, see Table 1 for transducer locations. One of the driven section channel segments is equipped with glass windows for flow visualization. A single-pass shadowgraph system is used in connection with a Photron SA5 high-speed video camera to record the shock trajectory and the particle cloud movement. In some cases, a front-lit, direct video was taken when passing parallel light through the optical section was not possible. The camera is triggered when the shock wave reaches location P3. The camera field-of-view covers half the length of the optical section window shown in Fig. 1.

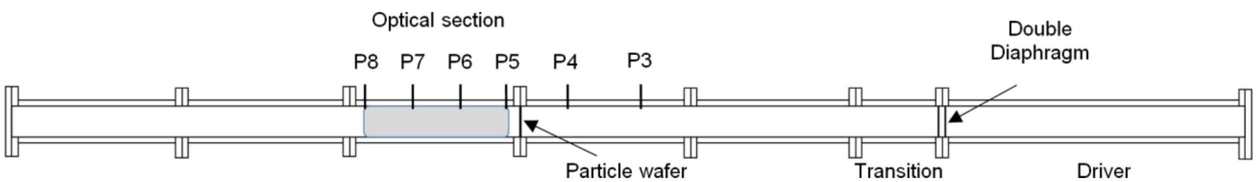

Figure 1. Schematic of shock tube showing the positions of the wafer, optical section, and the pressure transducers

Table 1. Pressure transducer distances from diaphragm

Transducer	P3	P4	Particle Wafer	P5	P6	P7	P8
Distance (m)	1.511	1.816	1.969	2.051	2.203	2.356	2.508

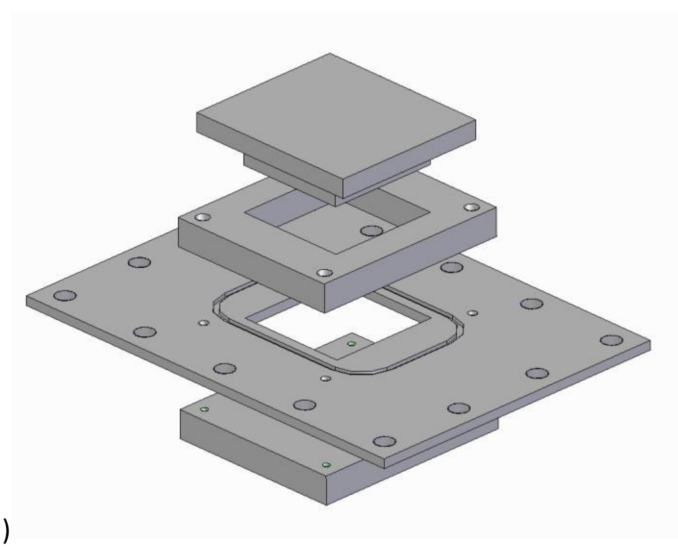
(a)
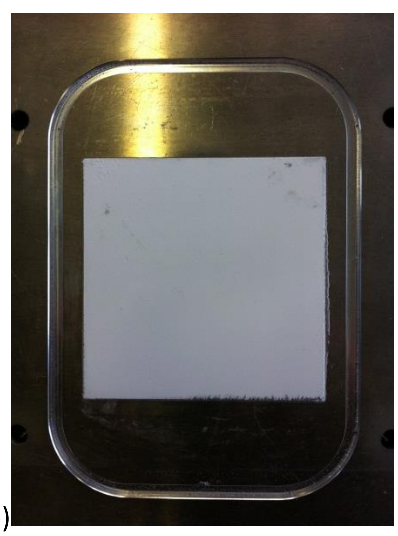
(b)

Figure 2. **a.** Die used to compress powder into the plate cavity **b.** particle wafer loaded in the plate}

The particles are initially configured in a wafer that is located between P4 and P5, as seen in Fig. 1, 1.97 m downstream of the diaphragm and 8.5 cm upstream of the edge of the optical section window. The particle wafer is created by compressing 70 g of aluminum oxide powder into a 7.6 cm square cavity machined into a 6.4 mm thick plate. The aluminum oxide is compressed using a 75 ton hydraulic press that compresses the powder into the plate cavity using the die shown schematically in Fig. 2a. A photograph showing the wafer in the plate cavity is shown in Fig. 2b.

As shown in Fig. 1, the plate containing the powder wafer is sandwiched between two flanges such that the cavity lines up with the channel cross-section area. This ensures that the particle wafer uniformly fills the entire shock tube cross-section such that no air bypass is possible following shock reflection. The initial position of the wafer between flanges makes it impossible to capture the initial shock and particle wafer interaction using the shadowgraph video system. Attempts to slide the wafer into the optical section field-of-view near P5 resulted in unacceptable gaps forming between the wafer and the inner-channel walls. The wafer has a particle volume fraction $\Phi = 0.48$ and the aluminum oxide powder has a mean particle diameter of 100 μm.

Videos were processed using the computer program *ImageJ* to create binary black-and-white frames using a color threshold to define the cloud area. The binary images where then processed using a code developed in *MATLAB* that allowed for the tracking of the particle cloud position. The cloud front referred to in this paper was defined as the average of the leading and trailing edges of the front.

Results and Discussion

Delrin® Block

Reference tests were performed with a loose-fitting solid Delrin® block placed in the same location as the particle wafer. The block was of the same mass as the particle wafer and was inserted inside the channel. The data from one such experiment with a driver pressure of 11 bar absolute is provided in Fig. 3. The pressure traces recorded at P3 through P8 (see Fig. 1 for transducer locations) are shown in Fig. 3. The reference of all pressure transducers is ambient atmospheric pressure (initial driven section pressure). Also shown are the high-speed video captured trajectories of the block and the shock wave that forms downstream. The incident shock wave reflects off the upstream side of the block producing a reflected shock wave that propagates back towards the driver section. The reflected shock wave corresponds to the second pressure rise in the pressure signals recorded at P3 and P4 in Fig. 3. A straight dotted line connects points on P3 and P4 (corresponding to shock time-of-arrival) showing the average trajectory of the incident and reflected shock wave. The 695 m/s (Mach number equal to 2) incident shock wave produces a 311 m/s and 14.5 bar reflected shock wave immediately after reflection that subsequently accelerates as it passes through the contact surface. This compares to theoretical fixed-surface normal reflection values of 348 m/s and 15.2 bar. The deviation could be attributed to the block acceleration and high pressure air leakage past the block due to a loose fit. The interaction of the shock wave with the block results in acceleration of the block to a relatively constant velocity of 204 m/s. The piston-like motion of the block produces a weak shock wave that propagates at a velocity of 391 m/s. The weak precursor shock wave could also originate from the small amount of gas that initially bypasses the block around the edges. The acceleration of the block and bypassing of some of the reflected shock gas produces a shallow pressure gradient between the block and the precursor shock wave. The high pressure air behind the block moves downstream with the block that is manifested as a travelling shock-like pressure pulse observed in the P5 to P8 signals in Fig. 3. The pressure behind the block decays as the block propagates down the channel and the high pressure gas region expands as the distance between the block and the reflected shock increases.

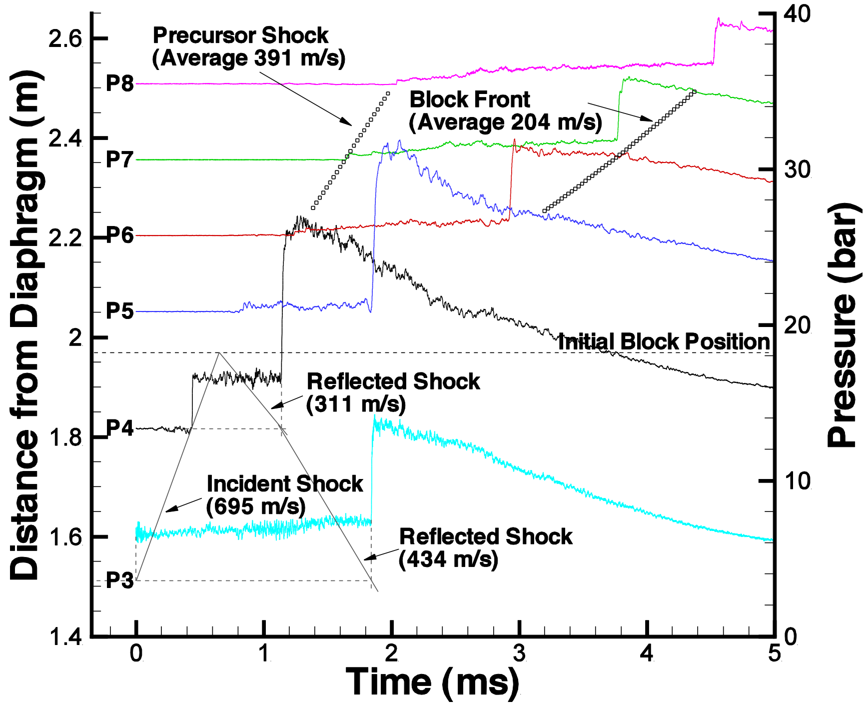

Figure 3. Diagram showing pressure traces as well as shock and block trajectories for an 11 bar abs. helium driver.

Particle Wafer - Square Cross-section

Results with the particle wafer obtained from two tests performed with a 6.5 bar absolute driver pressure and atmospheric pressure in the driven section is shown in Fig. 4. The camera field-of-view for the test results in Fig. 4a consists of the first half of the window, see Fig. 1. For the results shown in Fig. 4a, the incident shock wave velocity measured from the shock time-of-arrival between P3 and P4 is 581 m/s. The incident shock wave reflects off the particle wafer producing a reflected shock wave that propagates back at an average velocity of 316 m/s. The pressure behind the reflected shock wave measured at P4 remains relatively constant at about 8.5 bar over a period of roughly 0.4 ms, after which time the pressure starts to drop off. Based on the incident shock wave velocity, the theoretical reflected shock velocity and pressure that would be produced upon reflection from a solid immobile surface are

333 m/s and 8.4 bar, respectively. The close correspondence between the measured and theoretical reflected shock parameters, similar in magnitude with the block test shown in Fig. 3, indicates that the back of the wafer remains largely intact after the reflection and there is very little initial forward movement of the wafer over this time. When the wafer starts to move forward, expansion waves propagate back towards the reflected shock wave dropping the pressure along the way. By the time the reflected shock wave reaches P3 the head of the expansion has caught the shock wave and the pressure behind the shock wave drops immediately. The initial slow forward motion of the wafer produces compression waves that move ahead of the wafer. This causes the pressure at transducer P5 to rise slowly. A pressure front forms at P6 that steepens with distance as the compression waves merge. At P8, the compression waves have coalesced to form a shock wave characterized by a steep pressure rise at roughly 3 ms in Fig. 4a.

As long as the back edge of the particle wafer remains intact, it acts like a piston driven by the high pressure produced by the reflection of the incident shock wave. The passage of the rear edge of the wafer therefore passes P5 at 2.2 ms in Fig. 4a when a large pressure rise is recorded. The finite pressure rise-time recorded at P5 indicates that the back of the wafer is not completely intact and that there is some high pressure air bypassing the wafer. The pressure pulse propagates forward at a velocity slower than the precursor shock wave and the magnitude of the pressure pulse dramatically decreases with distance. Also shown in Fig. 4a is the position of the front edge of the particle cloud taken from high-speed video images shown in Fig. 5. The front edge of the cloud, defined as the average between the leading and trailing edges of the cloud front, moves at a velocity of 250 m/s. From Fig. 4a it is clear that the front edge of the cloud passes the transducer P5 position before the large pressure pulse, which is associated with the passage of the back edge of the particle cloud. More importantly is the fact that the distance between the front edge and back edge (deduced from the pressure pulse) of the cloud increases with propagation distance.

Shown in Fig. 5 is a compilation of high-speed video images taken from the two tests represented by Fig. 4. The initial wafer location is 8.5 cm beyond the right edge of the field-of-view. Time zero corresponds to the elapsed time after the shock wave reaches the P3 location shown in Fig. 1. As the cloud front edge moves forward, a weak compression wave forms that eventually is reinforced to form a shock wave by the left edge of the field-of-view, corresponding to the transducer P8 location in Fig. 1. The back edge of the cloud is not viewable because particles are trapped in the slow moving boundary layer flow next to the windows. Particles acquire a static charge during their motion and adhere to the glass windows. The position of the front edge of the particle cloud and the forming shock wave obtained from the video images from a test where the camera field-of-view covers the second half of the window is plotted in Fig. 4b. The velocity of the compression waves obtained from the video images is 472 m/s. The compression wave position obtained from the video agrees very well with the pressure rise recorded at P7 and P8. The video images indicate that the front edge of the cloud propagates at a velocity of 248 m/s. This measured cloud front edge velocity is higher than the theoretical post-shock gas velocity of 181 m/s behind the 472 m/s precursor shock wave.

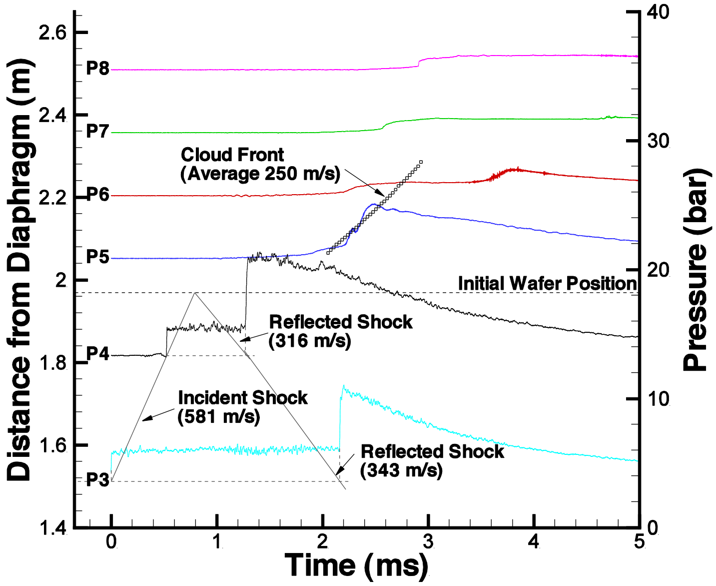

(a)

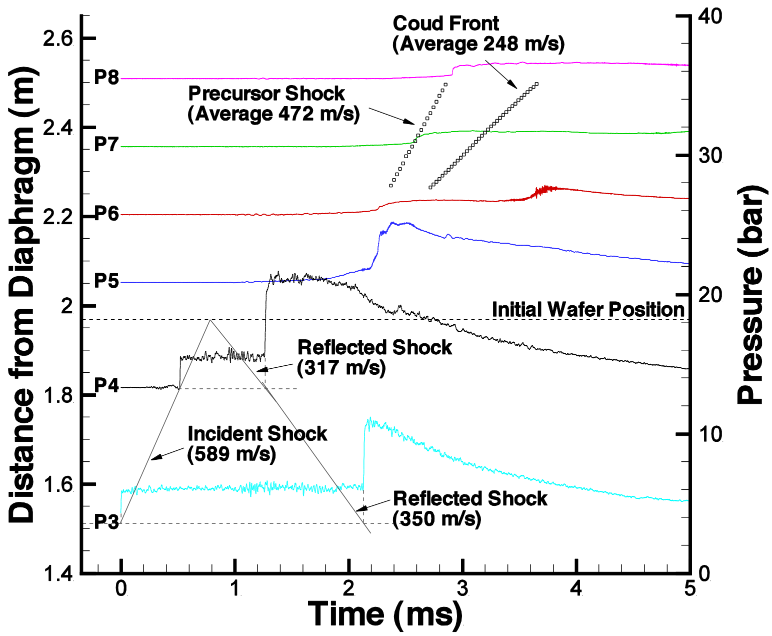

(b)

Figure 4. Diagram showing pressure traces for 6.5 bar abs. helium driver. Shock and block trajectories with the camera field-of-view covering **a.** the first half of the optical section **b.** the second half of the optical section.

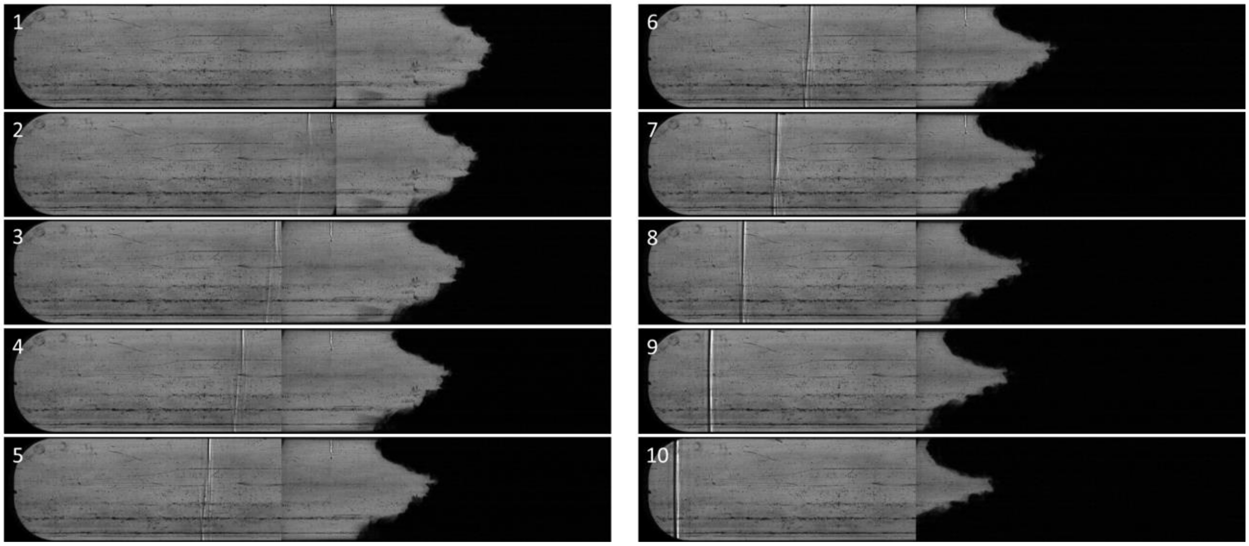

Figure 5. Compilation of two videos showing the non-uniform particle cloud leading-edge and the shock wave development ahead of the particle cloud. From tests with 6.5 bar abs. helium driver. Inter-frame time is 0.027 ms. Shock wave propagation is from right to left.

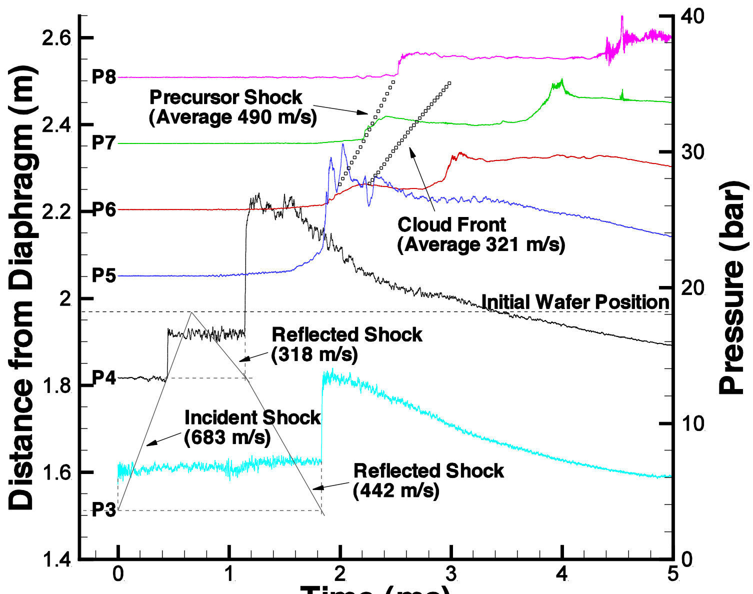

(a)

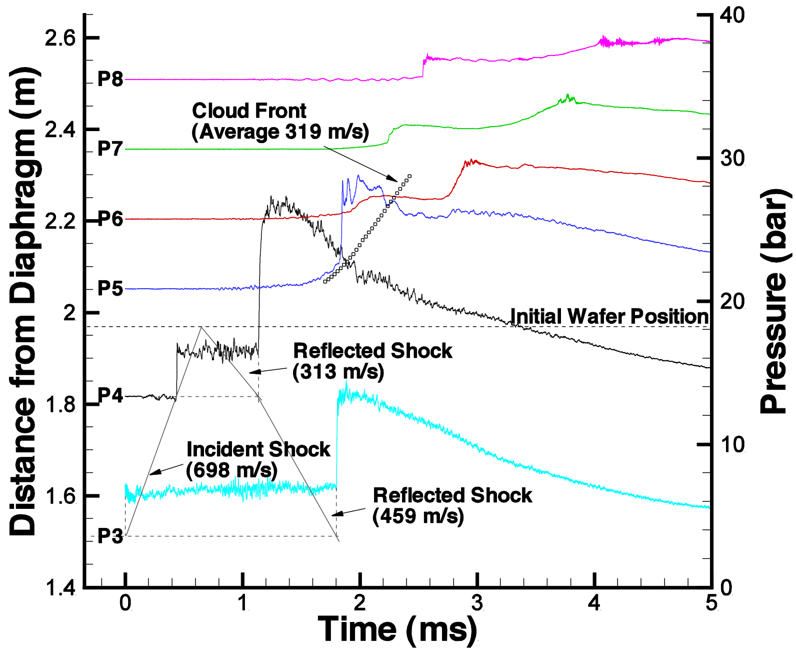

(b)

Figure 6. Diagram showing pressure traces for 11 bar abs. helium driver. Shock and block trajectories with the camera field-of-view covering **a.** the first half of the optical section **b.** the second half of the optical section}

Results obtained from tests performed with an 11 bar absolute driver pressure and atmospheric pressure in the driven section are shown in Fig. 6. The test results in Fig. 6a show an incident shock velocity of 698 m/s is produced. The reflected shock pressure at P4 is 14 bar, which is lower than the theoretical value of 15.6 bar. The motion of the wafer produces a shock wave velocity of 507 m/s measured between P7 and P8 (not shown in Fig. 6a). Between transducers P6 to P8, the precursor shock wave is followed by a well-defined pressure rise associated with the back edge of the particle cloud. As observed in the 6.5 bar driver tests shown in Fig. 4, the pressure rise-time increases as the wafer develops into a dense particle cloud. Based on the video, the velocity of the front of the cloud is 319 m/s, which again is significantly faster than the theoretical particle velocity of 233 m/s behind the 515 m/s precursor shock wave. The arrival of the back edge of the cloud can be inferred from the arrival of the second pressure pulse at P6, P7 and P8. This is in contrast to the fast rise-time, shock-like pressure pulse associated with the moving solid block in Fig. 3. The pressure rise is spread out over the cloud thickness and the exact location of the cloud back edge must be after the pressure maximum due to expansion dispersion into rear flow. The data from a test performed under similar conditions where the camera field-of-view covers the second half of the window is provided in Fig. 6b. The arrival of the back edge of the cloud at P6 is again identified after the pressure maximum at 3 ms.

Cloud Front Shape

An interesting feature that can be seen in Fig. 5 is the non-uniform, inverted “V” shape of the cloud leading-edge that is produced. The non-uniform leading edge develops very quickly, as it is present when the particle cloud enters the field-of-view. As the cloud moves downstream, the depth of the cloud leading-edge trough increases. This indicates that the particles near the channel wall are moving faster than particles at the center of the channel. The cloud shape is surprising because boundary layer theory would predict a parabolic shaped velocity profile with a velocity deficit at the walls that the particles would be expected to follow. A series of tests were performed to resolve questions concerning the cloud front-edge shape. The top and bottom surface of the channel are aluminum that have a different surface finish than the glass sides. To address this asymmetry the aluminum plates were replaced with glass plates in order to make all the channel inner-surfaces similar. With all channel surfaces made of glass, the inverted “V” shaped profile persisted.

The cloud front-edge observed in Fig. 5 is in contrast to the planar cloud front-edge obtained by Wagner et al. [6]. Experiments were performed with a wafer that does not span the full width of the channel, a similar geometry to the particle curtain in Wagner et al. [6]. Therefore, it was thought that the corners of the square cross-section wafer used in the current experiment might be affecting the development of the cloud shape. A particle wafer was created with 12.7 mm cut away from the sides with a knife after the die was removed. Tests were performed with the two gaps positioned on either side or the top and bottom, as shown in Fig. 7, in order to visualize the asymmetric cloud dispersion.

The results obtained with the wafer in the orientation shown in Fig. 7a are provided in Fig. 8. The images show a uniform cloud leading-edge, with a cloud density gradient in the streamwise direction. The cloud leading-edge appears to be very diffuse with the density increasing towards the rear of the cloud. In the first three images a very thick shock is immediately observed following the shock-wafer interaction. This is in contrast with tests where the wafer fills the entire cross-section, see Fig. 5, where a shock wave forms far downstream. The shock wave that is observed ahead of the cloud in Fig. 8 is the incident shock wave that has bypassed the wafer through the cut-away edges. To confirm this, plan-view tests were performed with the wafer oriented as shown in Fig. 7b. The images captured with this different wafer orientation shown in Fig. 9 shows a much more complex shock wave structure and cloud particle distribution. The diffracted shock waves from either side of the wafer reflect at the centerline of the channel producing a Mach stem, seen in the first image in Fig. 9. The Mach stem grows with time as the two triple-points move in opposite directions. The shear layers originating at the two triple-points interact at the centerline of the channel. The shock wave structure develops over time where the transverse waves decay and the shock front becomes more planar. As the incident shock wave travels through the cut-away gaps the shear at the wafer edges strip away particles from the wafer. The stripped particles accumulate forming an elongated cloud in the recirculation downstream from the wafer. The side and plan view images in Figs. 8 and 9 are combined into a series of composite images in Fig. 10. The images in Fig. 10 give a full three-dimensional view of the development of the complex shock wave structure and the trailing particle cloud. The thick shock wave seen in the side view in Fig. 8 is an integrated effect of the diffracted shock waves and the Mach stems. Furthermore, the planar cloud leading-edge that appears in Fig. 8 masks the highly non-uniform particle cloud that forms downstream of the wafer that is observed in Fig. 9.

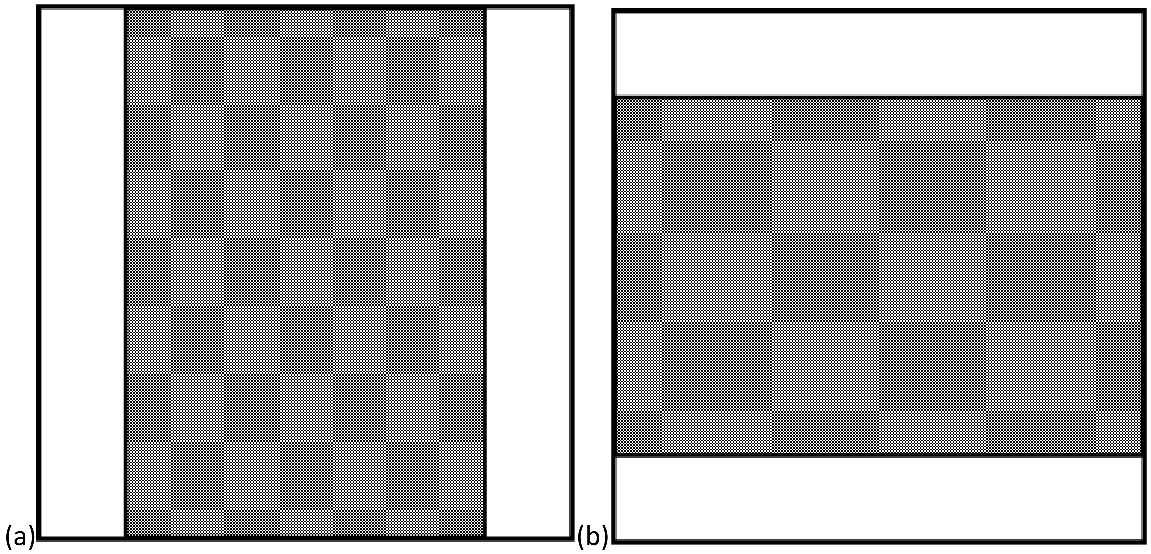

Figure 7. Modified particle wafer with 12.7 mm sidewall gaps **a.** vertically oriented **b.** horizontally oriented.

Since the wafer could not be placed in the field-of-view, the shock diffraction and early-time development of the wafer could not be visualized. In order to capture the early stage phenomenon, a Delrin® block of the same mass as the particle wafer was placed within the field of view, see Fig. 11. A layer of alumina powder was placed on the top edge of the block in order to determine the dispersion pattern of the particles sheared off the edge of the actual wafer. The images in Fig. 11 clearly show that there is no transmitted shock that passes through the block. In fact, over the 0.17 ms time elapsed for all the images in Fig. 11, the block does not move at all. The incident shock wave propagates through the gaps between the block edge and the channel side wall. The shock wave diffracts around the blocks two trailing-edges. The diffracted shock waves collide at the centerline at roughly 0.906 ms and proceed to form a roughly planar leading shock wave by 1.147 ms. The shock diffraction also forms a vortex that travels toward the channel centerline. The two vortices and the trailing shear layer eventually merge to form a turbulent recirculation zone behind the block. The powder on the top-edge of the block is very quickly mobilized, forming an elongated cloud that initially follows the shear layer, see the image at 0.987 ms. Over time, the cloud disperses and accumulates in the recirculation zone, see the image at 1.947 ms.

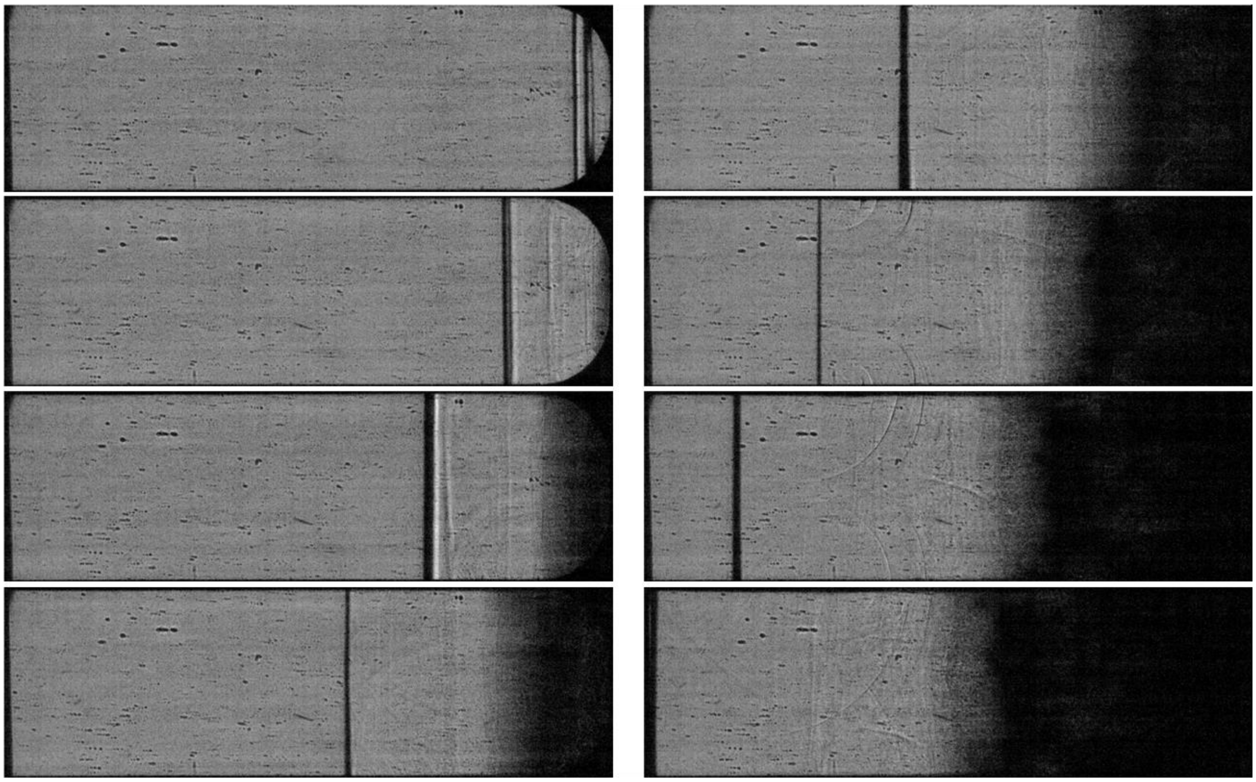

Figure 8. Images showing the shock wave and particle cloud dispersion. Results for 11 bar abs. driver pressure with 12.7 mm gap on sidewall wafer edges as shown in Fig. 7a. Shock wave propagation is from right to left.

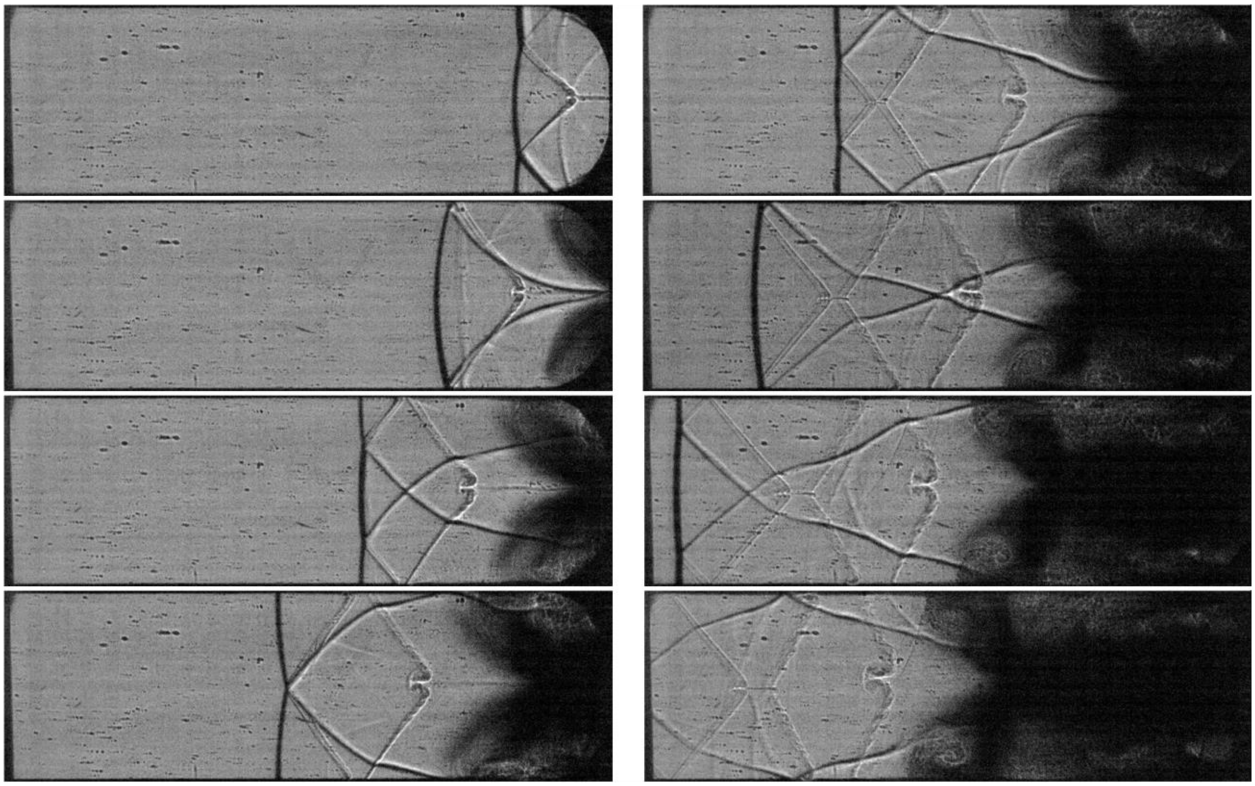

Figure 9. Images showing the shock wave and particle cloud dispersion. Results for 11 bar abs. driver pressure with 12.7 mm gap on sidewall wafer edges as shown in Fig. 7b. Shock wave propagation is from right to left.

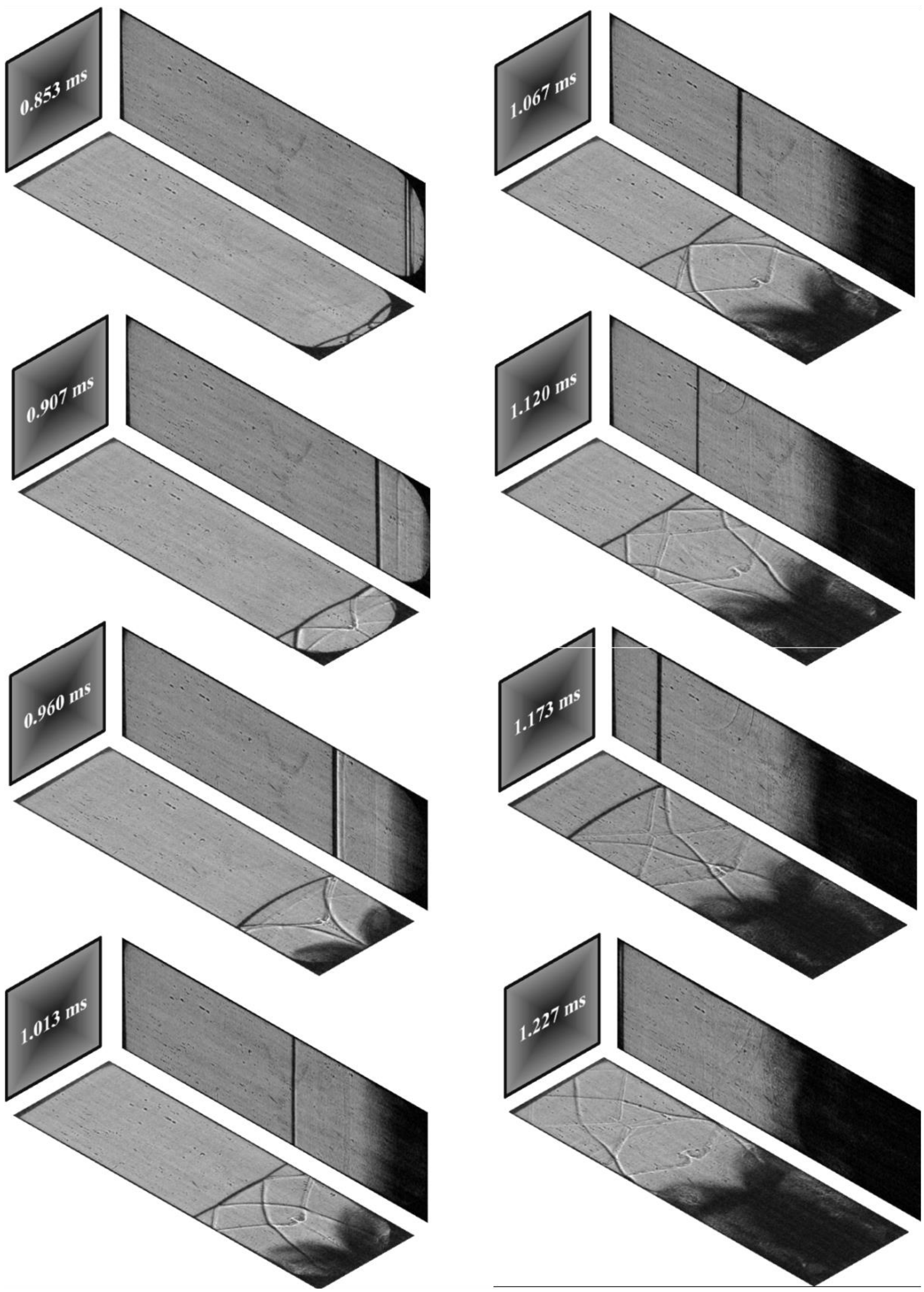

Figure 10. Composite image constructed from Figs. 8 and 9.

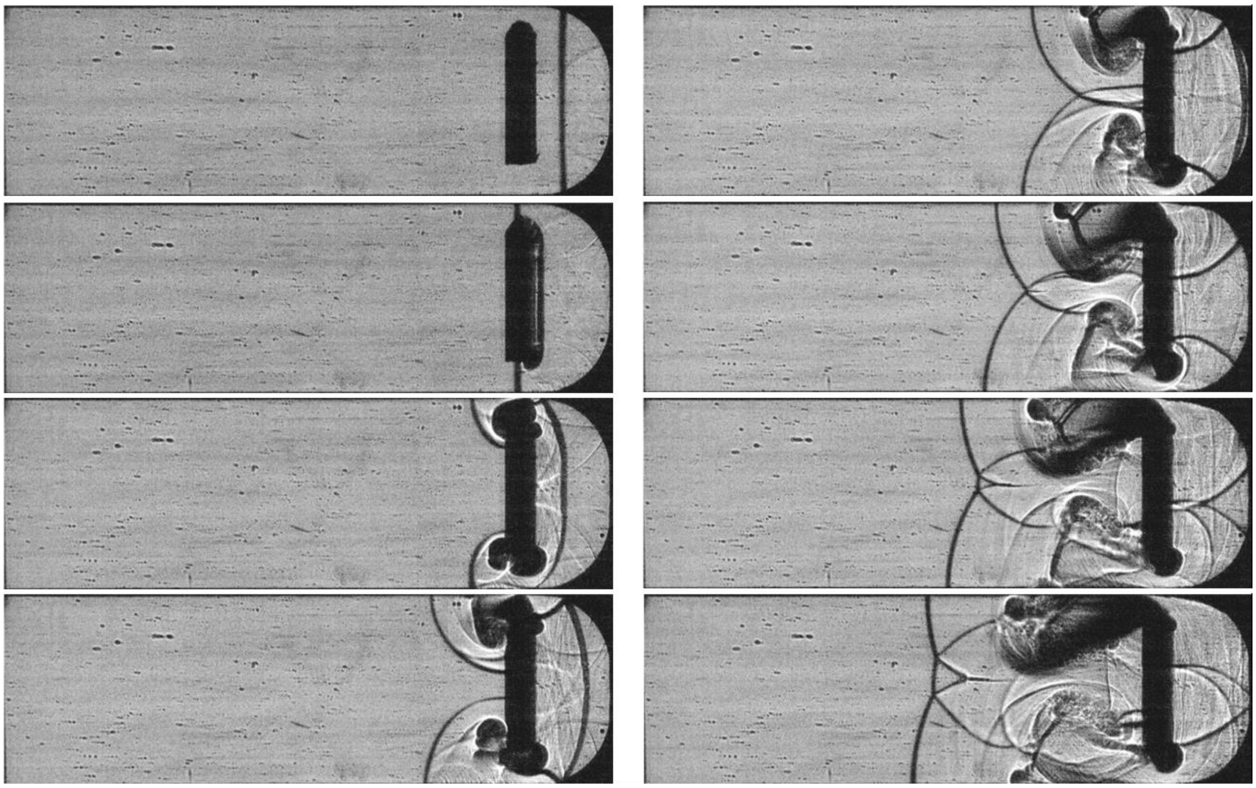
(a)
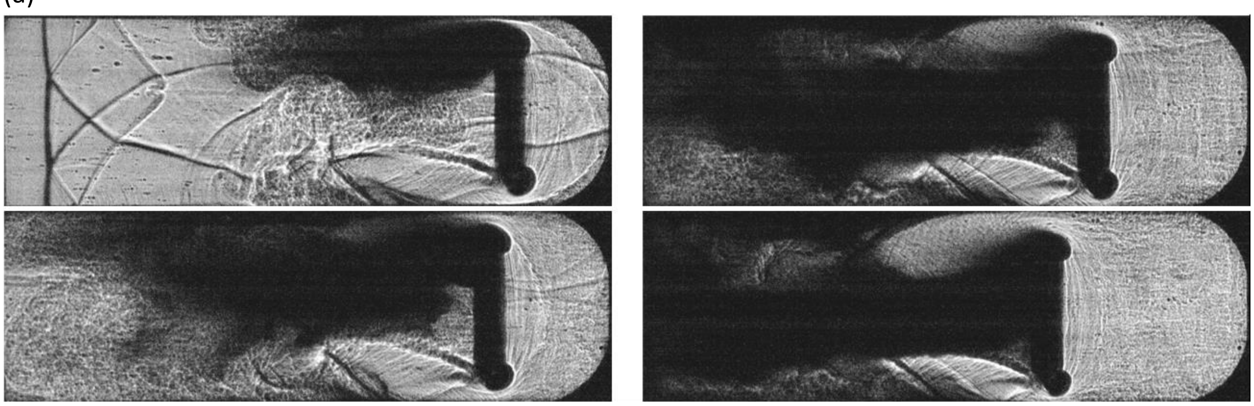
(b)

Figure 11. Images showing shock and particle dispersion from the top of a Delrin® block following the interaction of shock wave produced by 11 bar abs. driver (12.7 mm gap on top and bottom) **a.** initial interaction **b.** late time interaction. Shock wave propagation is from right to left.

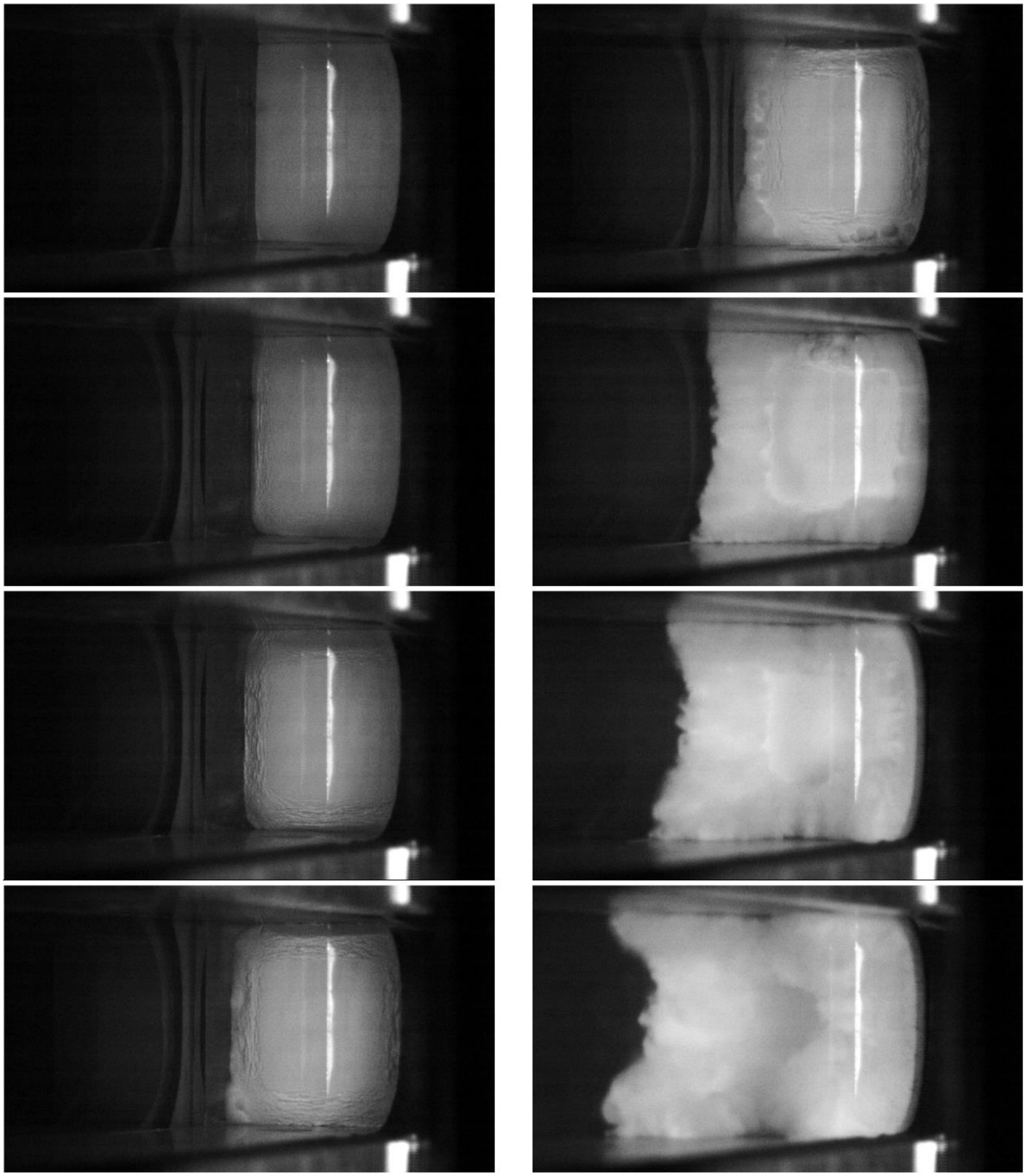

Figure 12. Images showing the initial wafer breakup and cloud development for 11 bar abs. driver pressure.

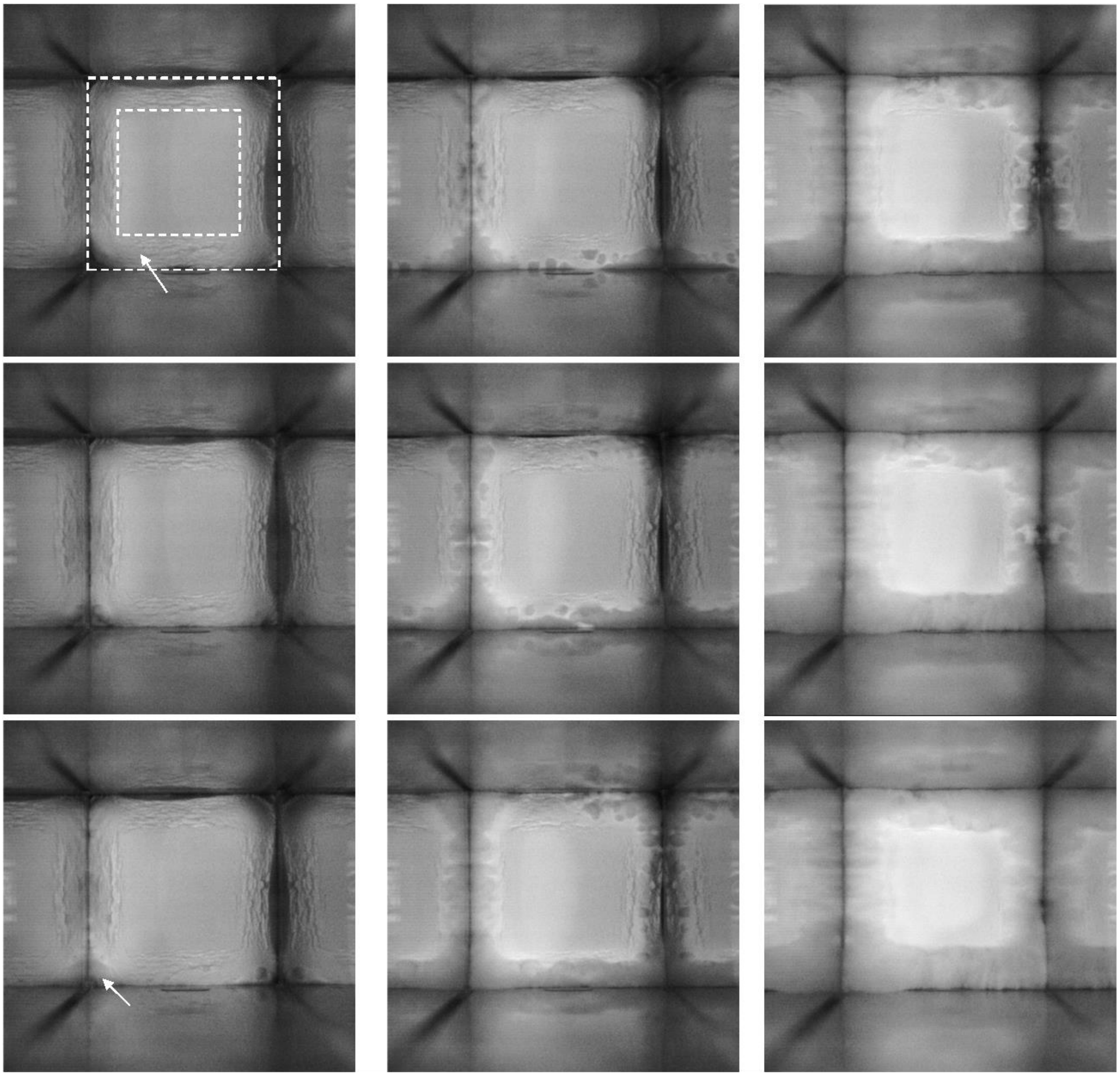

Figure 13. Head-on view showing initial wafer breakup and cloud development for 11 bar abs. driver pressure.

Downstream Surface Visualization

High-speed video of the wafer downstream surface was visualized in order to investigate the source of the non-uniform cloud leading-edge development. Moving the camera to approximately a 30° angle from the shock tube axis allowed the observation of the front of the wafer during the shock-wafer interaction. The interaction is observed in the front-lit direct video images in Fig. 12. The development of the non-uniform leading-edge of the particle cloud, observed from the side-view videos in Fig. 5, can now be seen in three-dimensions. The smooth surface of the wafer before the shock reflection can be seen in the first image at 1.033 ms. In the next image a perturbation develops around the wafer edge.

The corners of the wafer start to degenerate and accelerate ahead of the wafer edge starting at 1.433 ms. From this time on, it is clear that the particle cloud advances faster in the corners, clarifying the source of the non-uniform side-view images of the cloud in Fig. 5. The center of the wafer remains intact through the initial acceleration and is obscured by the leading edge of the particle cloud starting at 1.900 ms. As a result, it is not possible to observe the breakup of the center of the particle wafer. The vertical white sliver in Fig. 12 is light reflected off the front window.

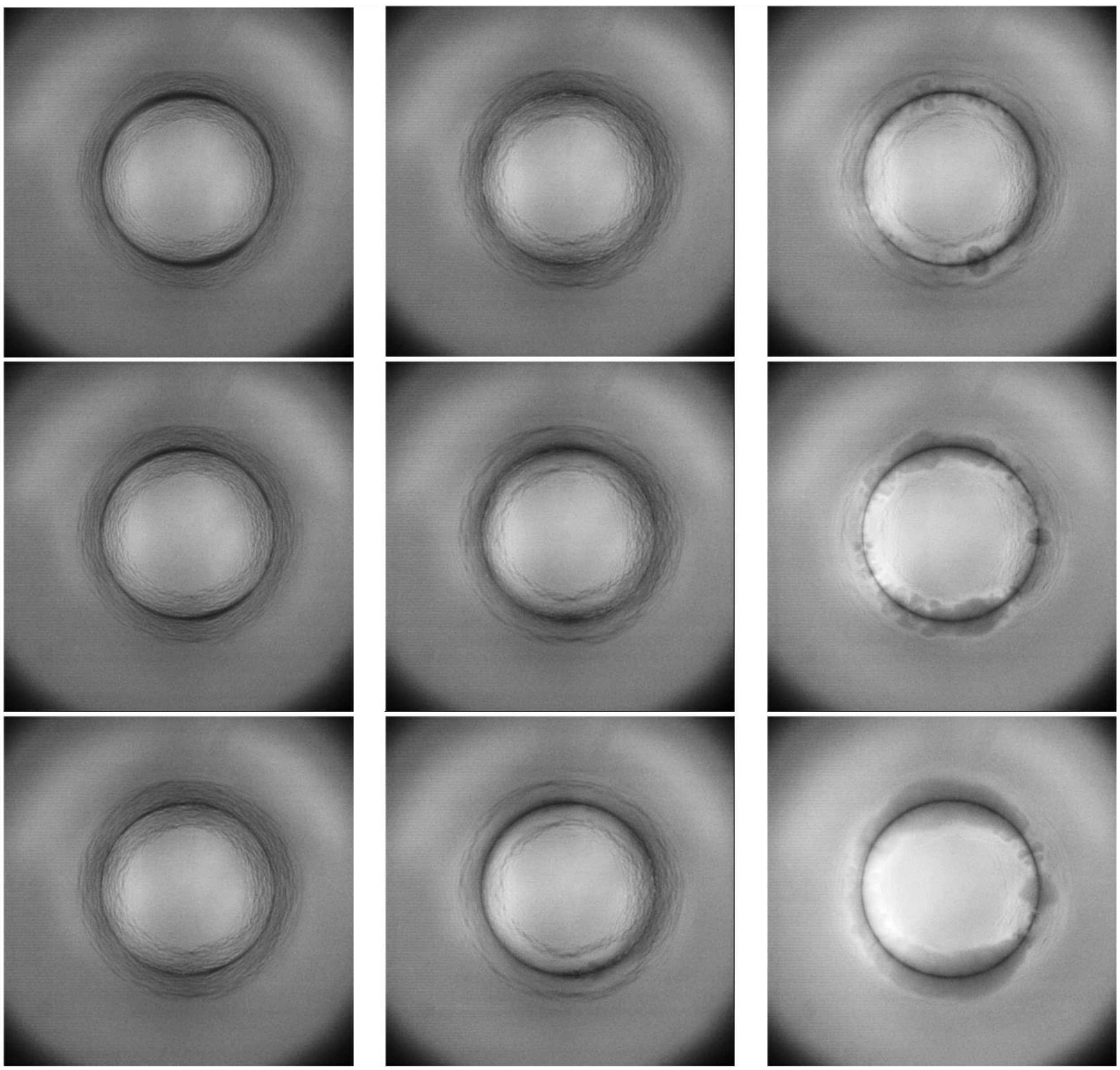

Figure 14. Head-on view showing initial wafer breakup and cloud development in a circular tube for 11 bar abs. driver pressure.

The use of an endplate with optical access enabled high-speed visualization of the wafer break up from a head-on perspective. The camera lens depth-of-field for this video was quite short with focus being lost after approximately 10 cm. The advantage of the camera view shown in Fig. 13 is that the wafer is visible in its entirety through the dispersion process.

As the wafer advances, following shock reflection, the edges lag behind the center and ripples form along the edges. The ripples represent a degradation of the integrity of the particle wafer structure. The lateral extent of the degradation zone around the edge does not change in time. The center of the wafer remains intact as it advances and is eventually obscured by the dispersed particles from the degradation zone. The first signs of wafer failure appear in the corners as darker areas in the images in Fig. 13. These dark areas correspond to particle jets that are first observed in the corners in Fig. 12. Particle jets start to form on the left and bottom edges at 2.871 ms, and then on the right and top edges at 2.935 ms.

The advancement of the center of the wafer and the fixed edge boundary condition leads to shear along the edges of the wafer. The shear causes slip between the particles and the wafer degrades locally. As the wafer center advances, the level of shear increases. The square geometry produces shear concentrations in the corners, leading to the primary locations for wafer failure. As a result, the high pressure air produced by the shock reflection is able to penetrate the wafer locally at these locations, producing the particle jets observed in the corners. As the wafer advances, the shear along the edges increases leading to additional failure locations. Interestingly, the failure along the wafer edge does not occur uniformly, but instead occurs locally forming discrete particle jets. These jets associated with the failure of the wafer are analogous with the jets that form in large-scale multiphase explosions [3, 8]. The spherical expansion of the solid explosives does not generate shear in the surrounding packed particle bed shell, instead the outward radial motion results in a circumferential tension in the particle shell. Based on the failure mode observed in the present wafer tests, it is possible that discrete failure points in the shell are the origins of the high-speed jets that are observed later in time.

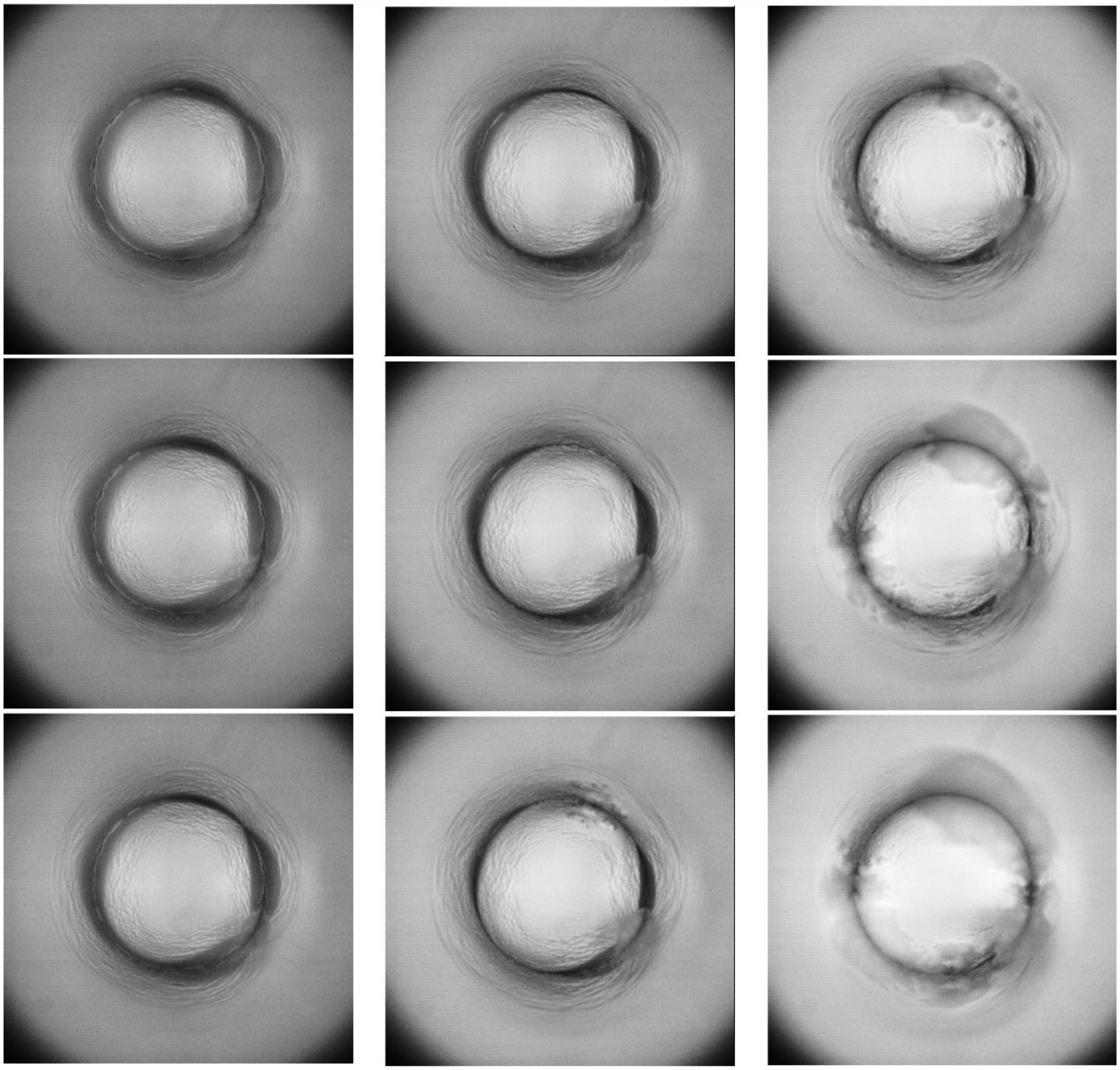

Figure 15. Head-on view for 11 bar abs. driver pressure showing initial wafer breakup in round cross-section with a pushed-in particle wafer.

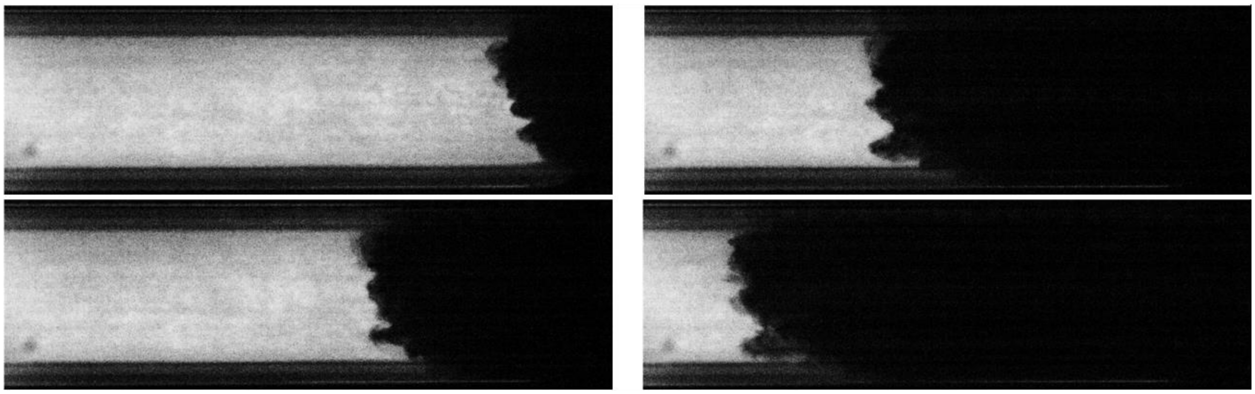

Figure 16. Particle cloud leading-edge for pushed-in wafer in round cross-section. Images are back-lit, directly shot. From tests with 11 bar abs. helium driver. Particle cloud propagation is from right to left.

Particle Wafer - Round Cross-section

From the downstream surface visualization, the corners were shown to fail first due to the meeting of two walls, along which a fixed boundary condition was present. At the corners, the boundary effect becomes enhanced due to the close proximity of two edges, creating an area of the wafer that is resistant to shear. Wafer failure occurs just inside of this point, towards the wafer center. By removing the corners present in a square cross-section with the use of a circular cross-section, a uniform boundary condition around the circumference was created. This was done by inserting tightly fitting 7.6 cm outer-diameter, 7.0 cm inner-diameter acrylic tubes into the channel on either side of the wafer. Due to light refraction through the round tube, shadowgraph images were not able to be obtained, so a back-lit, directly shot method was used. In addition, the inserted tube also blocked the pressure transducers, so no pressure data is available for this geometry. The same wafer loading technique shown in Fig. 1 was used, so the wafer characteristics are identical to the square channel experiments with no tube. The head-on view of the wafer failure in this round geometry is shown in Fig. 14. The round black line is the tube inner diameter and the disturbance outside this line is a reflection of light off the inner surface of the tube. Note the 7.0 cm inner-diameter of the tube is smaller than the 7.6 cm square wafer, so the shock wave punches a circular section out of the full square wafer. Therefore, the circular tube tests have a different wafer boundary condition than the square channel experiments where the wafer edge lines up with the channel inner-walls. Similar to that observed in the square channel, a degradation zone develops around the edge of the circular wafer. In this geometry, the local failure points, where the particle jets form, are uniformly distributed along the wafer circumference, see the 2.742 ms image in Fig. 14. This is different from the square channel tests where the failure points are primarily inside from the channel circumference, see images in Fig. 13 at 2.903 ms and 2.968 ms.

With the circular tube, it was possible to push a circular particle wafer into the tube at the beginning of the optical section. In this geometry the wafer is not compressed up against the side wall, as was the case in the square channel tests where the die is inserted between the flanges. A series of end-view images from a test is provided in Fig. 15. The free edges results in a larger degradation zone around the circumference, leaving a smaller diameter portion of the wafer intact. Particle jets form primarily along the tube inner-wall but some failure points form away from the tube wall. Overall the failure mode between the plate-mounted and the pushed-in wafers are very similar.

Images from the side view video corresponding to the pushed-in wafer test from Fig. 15 is shown in Fig. 16. The cloud front shape now appears to be much more uniform and the inverted "V" shape no longer persists.

The particle cloud leading-edge velocity obtained from side-view, back-lit regular video is shown in Fig. 17. As can be seen there is considerable scatter in the circular tube data but in general the cloud leading-edge velocity is similar for the two wafer mounting methods. The cloud leading-edge velocity for the square channel lies roughly 30 m/s higher than that observed in the circular tube. This data shows that the initial rate of acceleration over the first 8.5 cm, outside the camera field-of-view, is faster in the square channel resulting in a higher velocity at the start of the field-of-view. However, within the field-of-view the rate of acceleration in both geometries is similar. Since the pressure behind the wafer and the mass per unit area is the same, the difference in the acceleration over the first 8.5 cm can be attributed to the difference in the friction produced by the wafer edge degradation in the square and circular geometry. Taking a similar approach as with the square channel, a Delrin® disk of the same mass as the particle wafer was placed inside the tube. As seen in Fig. 17, the velocity of the square block and circular disk is almost identical and is lower than the particle wafer cloud leading-edge. The very different velocity history between the cloud leading-edge and the Delrin® block and disk is due to the failing of the wafer edges. The gas that first jets through the wafer quickly accelerates particles torn off the edges downstream. Therefore, the high-speed dispersed particles constitute the leading-edge of the cloud. Since the trailing-edge of the cloud cannot be detected in the videos, it is not possible to know the velocity of the intact central part of the accelerating wafer. It is very likely that the intact wafer core velocity is close to the slower block/disk velocity observed in Fig. 17.

Wafer Breakup

Shown in Fig. 18 is a simulated x-t diagram for a shock tube with the same driver length and an endplate located at the position of the particle wafer. The expansion fan, contact surface and incident shock wave trajectories were obtained from calculations performed using the CFD code *ANSYS Fluent 13*. Fluent's unsteady density-based solver was used to solve the one dimensional, compressible, inviscid, governing equations of motion. These equations were accompanied by the ideal gas law and were solved with 2nd order accuracy. Specific heats for air and helium were specified at 1005 J/kg and 5196 J/kg, respectively. A mass-weighted mixing law was applied at the contact surface to determine the binary mixture properties. A comparison between simulations with 0.5 mm and 1 mm grid node spacing confirmed that the results are independent of grid size. Also shown in Fig. 18 is the trajectory of the leading edge of the particle cloud taken from a test with an 11 bar abs. driver. Since the initial response of the wafer to the impact of the incident shock wave is not observed in the experiment the theoretical trajectory of a non-dispersing particle wafer, i.e., solid block, responding to a constant back pressure equal to the reflected shock pressure is provided. After diaphragm rupture the head of the expansion fan propagates at a velocity of 1020 m/s back upstream into the driver producing a 695 m/s (Mach 2.0) incident shock wave. The leading expansion reflects back downstream at approximately 2 ms and travels at 1198 m/s. The contact surface follows behind the incident shock wave at a velocity of 435 m/s. The incident shock wave reflects off the endplate, i.e., corresponding to the locations of the particle wafer in the experiment, at 2.8 ms. The reflected shock wave then interacts with the contact surface producing a transmitted shock wave and an expansion wave that propagates towards the particle wafer. From the theoretical and experimental trajectories it is clear that the particle cloud dispersion is not affected by the expansion or contact surface associated with the shock tube operation. Therefore, the observed particle cloud dispersion is solely governed by the interaction of the particle wafer with the incident shock wave.

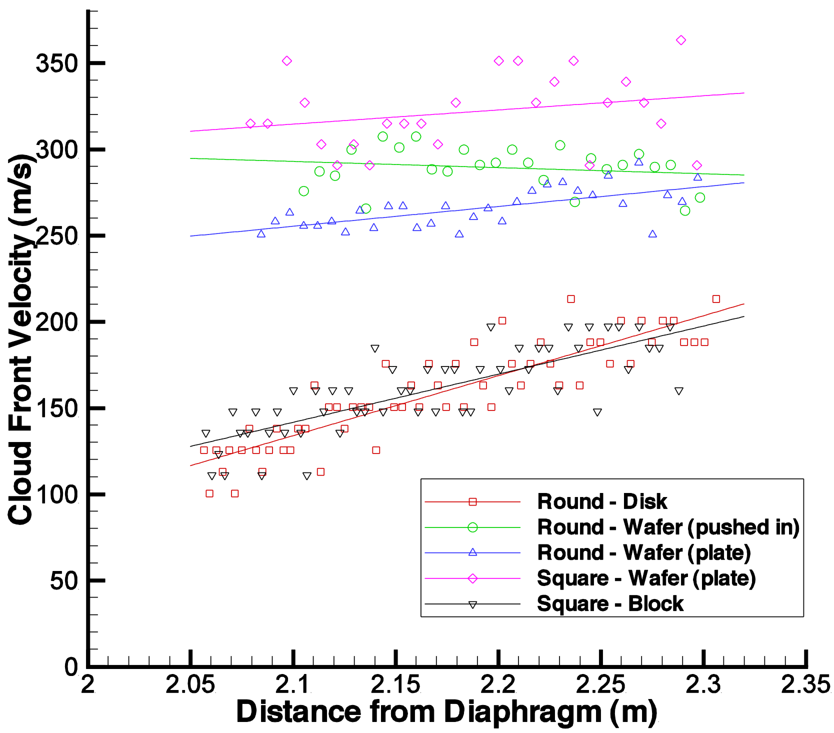

Figure 17. Experimental cloud front velocities from square and round cross-section.

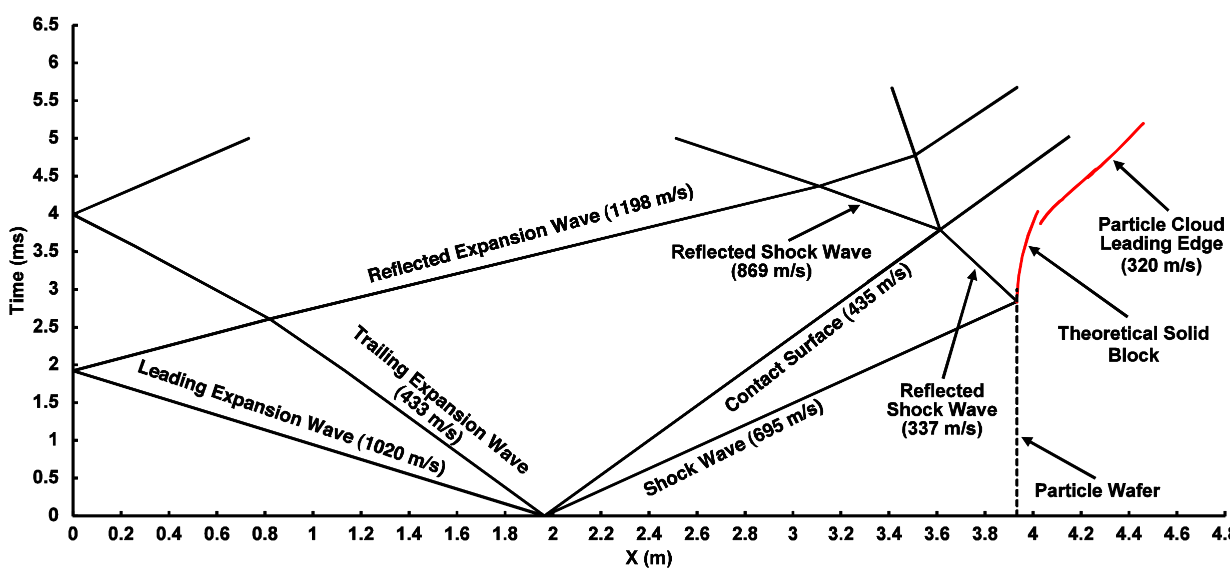

Figure 18. x-t diagram of the entire shock tube showing the arrival of each wave. Wave trajectories are taken from a CFD simulation and experimental data (red) is also shown. The CFD simulation was performed with a 10.8 bar abs. helium driver pressure, producing a 695 m/s incident shock wave in 1 atm air driven section. Experimental data taken from 11 bar abs. helium driver in 1 atm air driven section.

It is clear that the dispersion of a particle cloud with a high initial particle volume fraction (Φ = 0.48 for the wafer used in the present tests) is a multi-dimensional phenomenon. This is in contrast with the dispersion of a much lower Φ = 0.21 initial particle volume fraction cloud in the experiments performed by Wagner et al. [6]. At such a low particle volume fraction, the cloud consists primarily of gas and thus is relatively compressible compared to the wafer geometry that is pre-compressed to 254 bar. As a result, in the Wagner et al. particle curtain tests, the shock wave propagates through the curtain producing a dispersing cloud. The cloud dispersion occurs because the leading and trailing edges of the particle curtain can propagate at different velocities in response to the interaction of the incident shock wave with the leading-edge, and the precursor shock wave with the trailing edge. For the wafer, the Mach 2 incident shock wave is not able to compress the wafer and thus a shock wave does not propagate through the wafer. Instead, the wafer is accelerated uniformly and is dispersed by the failure of the wafer due to shear resulting from the boundary conditions. The wafer behaves much like a solid, so in order to have the leading and trailing edge of the wafer propagate at different velocities a shock pressure larger than the wafer pre-compression pressure is required. A stronger incident shock would accelerate the wafer leading-edge and the transmitted compression stress wave would reflect at the trailing-edge as a tensile stress wave. If the tension is higher than the effective wafer yield stress, a spallation process would ensue where particles would detach from the wafer trailing-edge. This spallation process would result in one-dimensional particle dispersion and edge boundary conditions would play a less important role in the wafer breakup, compared to that observed in the present experiments using a weak incident shock wave. Testing with stronger shock waves is not possible in the present shock channel due to the limiting strength of the glass windows.

It is important to note that the trailing-edge of the wafer is not visible from the side-view videos, since it is quickly obscured by the bypassing particles. Based on the end-view videos, the center of the wafer remains intact until it is obscured by edge particle coming in front of it. If spalling were to occur, it would be on a very short time-scale and it would be visible immediately after the shock-particle wafer interaction. Therefore, it is suspected that the wafer remains intact after the shock interaction and then is slowly eroded by the flow around the wafer.

Conclusions

Experiments were performed to observe the dispersion of an initially very dense particle cloud by a shock wave. The goal was to design a clean experiment where no supporting structures were used in the initial geometry of the particle cloud. The approach taken was to compress the particles into a free-standing wafer that could easily be positioned in the shock channel. The high particle volume fraction of the wafer resulted in a solid body response to the shock interaction. No transmitted shock through the particle wafer was observed. Breakup first occurs along the wafer edge in the degradation zone due to shear caused by the fixed wafer boundary condition. In a circular tube, failure of the wafer occurs as a series of particle jets that form along the wafer edge. In a square channel the failure first occurs in the corners, where the shear is enhanced, and then progresses to the edges. This failure mechanism produces a non-uniform cloud leading edge. In order to get a one-dimensional cloud dispersion using a particle-wafer, a shock wave capable of inducing spallation of the trailing-edge is needed.

References

1. Rudinger, G., Chang, A., Analysis of nonsteady two-phase flow, Physics of Fluids, 7(11), 1747–1755 (1964)
2. Zhang, F., Frost, D.L., Thibault, P.A., Murray, S.B., Explosive dispersal of solid particles, Shock Waves, 10(6), 431-443 (2001)
3. Zhang, F., Metalized heterogeneous detonation and dense reactive particle flow, AIP Conference Proceedings, 1426(1), 27-34 (2011)
4. Rogue, X., Rodriguez, G., Haas, J.F., Saurel, R., Experimental and numerical investigation of the shock-induced fluidization of a particles bed, Shock Waves, 8(1), 29-45 (1998)
5. Frost, D.L., Zhang, F., The nature of heterogeneous blast explosives, Proceedings of the 19th International Symposium on Military Aspects of Blast and Shock, (2006)
6. Wagner J., Baresh S., Kearney S., Trott W., Castaneda J., Pruett B., Baer M., Interaction of a planar shock with a dense field of particles, 28th International Symposium of Shock Waves, 2, 115-120 (2011)
7. Kellenberger, M., Johansen, C., Ciccarelli, G., Dense particle cloud dispersion by a shock wave, 28th International Symposium of Shock Waves, 2, 101-106 (2011)
8. Frost, D.L., Gregoire, Y, Goroshin, S., Zhang, F., Interfacial instabilities in explosive gas-particle flows, Proceedings of 23rd International Colloquium on the Dynamics of Explosions and Reactive Systems, Irvine CA (2011)